Lattice artifacts in the non-Abelian Debye screening mass in one-loop order

P. Kaste and H. J. Rothe
Institut für Theoretische Physik, Universität Heidelberg, Philosophenweg 16, D-69120 Heidelberg, Germany
(Received 23 May 1997)

We compute the electric screening mass in lattice QCD with Wilson fermions at finite temperature and chemical potential to one-loop order, and show that lattice artifacts arising from a finite lattice spacing result in an enhancement of the screening mass as compared to the continuum. We discuss the magnitude of this enhancement as a function of the temperature and chemical potential for lattices with a different number of lattice sites in the temporal direction that can be implemented in lattice simulations. Most of the enhancement is found to be due to the fermion loop contribution. [S0556-2821(97)03121-4]

PACS number(s): 11.15.Ha, 12.38.Gc

I. INTRODUCTION

An important feature of finite temperature QCD is the generation of electric and magnetic screening masses which play an important role in controlling the infrared behavior of the theory. The electric screening mass leads to a Debye-screened static quark-antiquark potential and is given for SU(N) with N_f quark flavors, and for vanishing chemical potential and quark mass, in leading order perturbation theory by $m_{\rm el}^2=(g^2/3)(N+N_f/2)T^2$ [1]. Renormalization-group-improved perturbation theory tells us that the effective coupling is a function of the temperature and decreases with increasing temperature. This suggests that at sufficiently high temperatures, above the deconfining phase transition, the screening mass may be computed in perturbation theory. Because of the singular infrared behavior of the perturbative series, however, the computation of the next to leading order contribution requires a resummation of infrared-divergent diagrams which turns out to be sensitive to the magnetic screening mass [2]. This mass vanishes in lowest order perturbation theory and is expected to be of $O(g^2T)$. The coefficient multiplying g^2T turns out, however, to be incalculable [3]. Making use of an improved perturbation theory proposed by Braaten and Pisarski [4], which resums hard thermal loops, and of a gauge-invariant definition of the electric screening mass [5], Rebhan has calculated the $O(g^3T^2)$ corrections to the non-Abelian screening mass squared and has shown that next to leading order contributions give rise to an enhancement [2].

The lattice formulation of QCD allows one to determine the electric screening mass nonperturbatively. The screening mass is extracted from correlators of Polyakov loops [6–9] or from the long distance behavior of the gluon propagator [10]. For small quark-antiquark separations lattice perturbation theory for the Polyakov loop correlation function is expected to describe the Monte Carlo data, since for a finite lattice volume one is not confronted with the infrared problems encountered in thermal perturbation theory. This has been checked in [11] for the SU(3) gauge theory by taking careful account of finite size effects and, in particular, of the zero momentum modes which do not allow one to take the thermodynamical limit for fixed coupling, as one would do in standard perturbation theory. For larger quark-antiquark separations, beyond the ''perturbative horizon,'' the color-averaged potential is expected to have a Debye screened form. Monte Carlo simulations confirm this screening picture [6–9]. In the case of pure SU(2) and SU(3) gauge theories the electric screening mass, when determined from Polyakov loop correlation functions, is found to be about 10% larger [6,7] than the leading order perturbative result if the temperature-dependent coupling constant is determined from Polyakov loop correlators in the perturbative region. As was pointed out by Rebhan [2], such an enhancement could also be expected if next to leading order corrections to the continuum screening mass are taken into account through resummed perturbation theory. A quantitative comparison with the results obtained in the above simulations is, however, very difficult and has, to our knowledge, not been carried out so far. In contrast to the work of Refs. [6, 7], the electric screening mass as extracted in Ref. [10] from the gluon propagator in the Landau gauge was found to deviate strongly from the leading order perturbative result.

In comparing the Monte Carlo data for the electric screening mass with leading order, or resummed, perturbation theory it is important to have an estimate of the size of lattice artifacts to be expected from a finite lattice spacing. To obtain such an estimate we compute the electric screening mass in one-loop order on the lattice, at finite temperature and chemical potential, and in the infinite volume limit, and compare it with the continuum. For the case of QED with *naive* fermions the screening mass has been calculated by Pietig [12]. The screening mass is calculated from the zero-momentum limit of the 44-component of the vacuum polarization tensor evaluated for vanishing Matsubara frequency. In one-loop order this definition of the screening mass is gauge invariant and consistent with the more general gauge-invariant definition given in Ref. [5], where the screening mass is determined from the position of the pole of the gluon propagator for vanishing Matsubara frequency.

The paper is organized as follows: In the following section we calculate the electric screening mass for QCD in one-loop order for the case of Wilson fermions. The Feynman rules and frequency summation formulas required for the computation are relegated to two Appendixes. As we shall see, the resulting integral expression has a very transparent form. In Sec. III we then evaluate the momentum integrals for the screening mass numerically and compare the results with the continuum. We show that the lattice artifacts

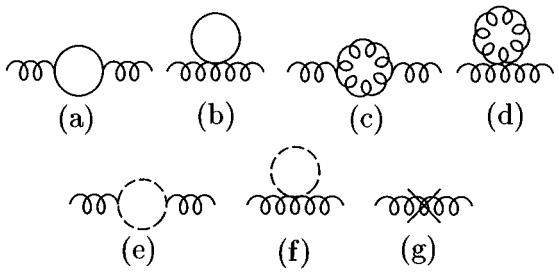

FIG. 1. Feynman diagrams contributing to the vacuum polarization in one-loop order on the lattice.

due to a finite lattice spacing give rise to an enhancement of the screening mass as compared to the continuum. We discuss the magnitude of this enhancement as a function of the temperature and chemical potential for lattices with a different number of lattice sites in the temporal direction which can be implemented in numerical simulations. Most of the enhancement is found to be due to the fermion loop contribution. Section IV contains a summary of our results.

II. ELECTRIC SCREENING MASS IN ONE-LOOP ORDER

In this section we compute the electric screening mass in lattice QCD to one-loop order from the zero momentum limit of the 44-component of the vacuum polarization tensor evaluated for vanishing Matsubara frequency. The Feynman diagrams contributing in this order are shown in Fig. 1. While diagrams (a), (c), (d), and (e) have a continuum analogue, the remaining diagrams, required by gauge invariance on the lattice, do not possess a continuum counterpart. The finite temperature, finite chemical potential lattice Feynman rules are obtained from the $T=\mu=0$ rules by replacing the fourth component of the fermion and boson momenta by $\hat{\omega}_l^- + i\hat{\mu}$ and $\hat{\omega}_l^+$, respectively, where $\hat{\omega}_l^+ = (2\pi/\hat{\beta})l[\hat{\omega}_l^- = (2l+1)\pi/\hat{\beta}]$, with $l \in Z$, are the Matsubara frequencies for bosons (fermions), and $\hat{\beta}$ is the inverse temperature. Quantities with a ''caret'' are always understood to be measured in lattice units. Furthermore, integrals over the fourth component of momenta at zero temperature are replaced at finite temperature by sums over Matsubara frequencies in the interval $[-\hat{\beta}/2, \hat{\beta}/2-1]$, where we have taken $\hat{\beta}$ to be even. The Feynman rules are collected in Appendix A. The relevant formulas for carrying out the sums over Matsubara frequencies are derived in Appendix B.

The contributions of diagrams (a)–(g) of Fig. 1 to the vacuum polarization tensor are diagonal in color space,

$$\hat{\Pi}_{\mu\nu}^{(\beta,\mu)AB}(\hat{\omega}_l^+, \vec{\hat{k}}) = \delta_{AB}\hat{\Pi}_{\mu\nu}^{(\beta,\mu)}(\hat{\omega}_l^+, \vec{\hat{k}}). \tag{2.1}$$

The electric screening mass (in lattice units) is then defined by

$$\hat{m}_{\rm el}^2 = \lim_{\vec{\hat{k}}\to 0} \hat{\Pi}_{44}^{(\beta,\mu)}(0,\vec{\hat{k}}). \tag{2.2}$$

In the following we first consider the contributions to $\hat{\Pi}_{44}^{(\beta,\mu)}(0,\vec{\hat{k}})$ coming from the fermion loops, i.e., diagrams (a) and (b).

A. Contribution of diagram (a)

A straightforward application of the finite temperature, finite chemical potential lattice Feynman rules yields

$$\hat{\Pi}_{44}^{(\beta,\mu)}(0,\vec{\hat{k}})_{(a)} = -\frac{N_f}{2} g^2 \frac{1}{\hat{\beta}} \sum_{l=-\hat{\beta}/2}^{\hat{\beta}/2-1} \int_{-\pi}^{\pi} \frac{d^3\hat{p}}{(2\pi)^3} \times f^{(a)}(e^{i(\hat{\omega}_l^- + i\hat{\mu})}; \vec{\hat{p}}, \vec{\hat{k}}), \tag{2.3a}$$

where

$$f^{(a)}(z;\vec{\hat{p}},\vec{\hat{k}}) = \frac{2(z^4+1) - 2\eta(z^3+z) + 4\xi\mathcal{G}z^2}{\Pi_{i=1}^4 (z-z_i)} \tag{2.3b}$$

with

$$\eta = \frac{1}{[1+\hat{M}(\vec{\hat{p}})]} + \frac{1}{[1+\hat{M}(\vec{\hat{p}}+\vec{\hat{k}})]}, \tag{2.3c}$$

$$\xi = \frac{1}{[1+\hat{M}(\vec{\hat{p}})][1+\hat{M}(\vec{\hat{p}}+\vec{\hat{k}})]}, \tag{2.3d}$$

$$\mathcal{G} = 1 + \sum_j \sin\hat{p}_j \sin(\hat{p}+\hat{k})_j, \tag{2.3e}$$

$$\hat{M}(\vec{\hat{p}}) = \hat{m} + 2\sum_j \sin^2\frac{\hat{p}_j}{2}, \tag{2.3f}$$

and N_f is the number of quark flavors. The position of the poles of $f^{(a)}(z;\vec{\hat{p}},\vec{\hat{k}})$ are given by

$$z_1 = e^{\phi}, \quad z_2 = e^{-\phi}, \quad z_3 = e^{\psi}, \quad z_4 = e^{-\psi}, \tag{2.4a}$$

with

$$\phi = \tilde{\mathcal{E}}(\vec{\hat{p}}), \quad \psi = \tilde{\mathcal{E}}(\vec{\hat{p}}+\vec{\hat{k}}), \tag{2.4b}$$

where

$$\tilde{\mathcal{E}}(\vec{\hat{q}}) = \ln[K(\vec{\hat{q}}) + \sqrt{K^2(\vec{\hat{q}})-1}] = \operatorname{arcosh} K(\vec{\hat{q}}) \tag{2.4c}$$

and

$$K(\vec{\hat{q}}) = 1 + \frac{\overline{E^2}(\vec{\hat{q}})}{2[1+\hat{M}(\vec{\hat{q}})]}, \quad \overline{E}(\vec{\hat{q}}) = \sqrt{\sum_j \sin^2\hat{q}_j + \hat{M}^2(\vec{\hat{q}})}. \tag{2.4d}$$

Note that

$$\phi \overset{\vec{p}\to-\vec{p}-\vec{k}}{\leftrightarrow} \psi, \tag{2.5}$$

while η, ξ, and $\mathcal{G}$ are invariant under the transformation $\vec{p}\to-\vec{p}-\vec{k}$. This will be important further below. The frequency sum can be performed making use of Eq. (B4) derived in Appendix B. One finds that

$$\begin{aligned}\frac{1}{\hat{\beta}}\sum_{l=-\hat{\beta}/2}^{\hat{\beta}/2-1} f^{(\mathrm{a})}(e^{i(\hat{\omega}_l^- + i\hat{\mu})};\vec{\hat{p}},\vec{\hat{k}}) &= 2 + h(\phi,\psi,\eta,\xi,\mathcal{G})\left[\frac{1}{e^{\hat{\beta}(\phi+\hat{\mu})}+1} - \frac{1}{e^{-\hat{\beta}(\phi-\hat{\mu})}+1}\right] \\ &\quad + h(\psi,\phi,\eta,\xi,\mathcal{G})\left[\frac{1}{e^{\hat{\beta}(\psi+\hat{\mu})}+1} - \frac{1}{e^{-\hat{\beta}(\psi-\hat{\mu})}+1}\right],\end{aligned} \tag{2.6a}$$

where

$$h(\phi,\psi,\eta,\xi,\mathcal{G}) = \frac{\cosh 2\phi - \eta\cosh\phi + \xi\mathcal{G}}{\sinh\phi(\cosh\phi-\cosh\psi)}. \tag{2.6b}$$

To obtain $\hat{\Pi}_{44}^{(\beta,\mu)}(0;\vec{\hat{k}})_{(\mathrm{a})}$, we must integrate this expression over $\vec{\hat{p}}$, with $\hat{p}_j\in[-\pi,\pi]$. Noting that η, ξ, and $\mathcal{G}$ are invariant under the transformation $\vec{\hat{p}}\to-\vec{\hat{p}}-\vec{\hat{k}}$, and making use of Eq. (2.5), as well as of the fact that the integrand in Eq. (2.3a) is a periodic function in $\hat{p}_j$ and $\hat{k}_j$, we can combine the last two contributions on the right-hand side (RHS) of Eq. (2.6a) and obtain

$$\begin{aligned}\hat{\Pi}_{44}^{(\beta,\mu)}(0,\vec{\hat{k}})_{(\mathrm{a})} &= N_f g^2\int_{-\pi}^{\pi}\frac{d^3\hat{p}}{(2\pi)^3}[h(\phi,\psi,\eta,\xi,\mathcal{G})-1] \\ &\quad - N_f g^2\int_{-\pi}^{\pi}\frac{d^3\hat{p}}{(2\pi)^3}h(\phi,\psi,\eta,\xi,\mathcal{G})[\,\hat{\eta}_{\mathrm{FD}}(\phi) + \overline{\hat{\eta}}_{\mathrm{FD}}(\phi)],\end{aligned} \tag{2.7a}$$

where

$$\hat{\eta}_{\mathrm{FD}}(\phi) = \frac{1}{e^{\hat{\beta}(\phi-\hat{\mu})}+1}, \quad \overline{\hat{\eta}}_{\mathrm{FD}}(\phi) = \frac{1}{e^{\hat{\beta}(\phi+\hat{\mu})}+1} \tag{2.7b}$$

are the lattice Fermi-Dirac distribution functions for particles and antiparticles.

B. Contribution of diagram (b)

We next compute the contribution to $\hat{\Pi}_{44}^{(\beta,\mu)}(0,\vec{\hat{k}})$ of the Feynman diagram (b) depicted in Fig. 1. This diagram has no analogue in the continuum and is given by

$$\begin{aligned}\hat{\Pi}_{44}^{(\beta,\mu)}(0,\vec{\hat{k}})_{(\mathrm{b})} &= -N_f g^2\frac{1}{\hat{\beta}}\sum_{l=\hat{\beta}/2}^{\hat{\beta}/2-1}\int_{-\pi}^{\pi}\frac{d^3\hat{p}}{(2\pi)^3} \\ &\quad\times f^{(\mathrm{b})}(e^{i(\hat{\omega}_l^- + i\hat{\mu})},\vec{\hat{p}}),\end{aligned} \tag{2.8a}$$

where

$$f^{(\mathrm{b})}(z;\vec{\hat{p}}) = -\frac{z^2-2\rho z+1}{(z-z_1)(z-z_2)}, \tag{2.8b}$$

$$\rho = \frac{1}{1+\hat{M}(\vec{\hat{p}})}, \tag{2.8c}$$

and where z_1 and z_2 have been defined in Eqs. (2.4). Making again use of the frequency summation formula (B4), one verifies that

$$\begin{aligned}\hat{\Pi}_{44}^{(\beta,\mu)}(0,\vec{\hat{k}})_{(\mathrm{b})} &= -N_f g^2\int_{-\pi}^{\pi}\frac{d^3\hat{p}}{(2\pi)^3}\left(\coth\phi - \frac{\rho}{\sinh\phi} - 1\right) \\ &\quad + N_f g^2\int_{-\pi}^{\pi}\frac{d^3\hat{p}}{(2\pi)^3}\left(\coth\phi - \frac{\rho}{\sinh\phi}\right) \\ &\quad\times[\,\hat{\eta}_{\mathrm{FD}}(\phi) + \overline{\hat{\eta}}_{\mathrm{FD}}(\phi)].\end{aligned} \tag{2.9}$$

Combining this expression with Eq. (2.7a) one finds that

$$\begin{aligned}\hat{\Pi}_{44}^{(\beta,\mu)}(0,\vec{\hat{k}}) &= \hat{\Pi}_{44}^{(\mathrm{vac})}(0,\vec{\hat{k}}) \\ &\quad + N_f g^2\int_{-\pi}^{\pi}\frac{d^3\hat{p}}{(2\pi)^3}H(\phi,\psi,\rho,\eta,\xi,\mathcal{G})[\,\hat{\eta}_{\mathrm{FD}}(\phi) \\ &\quad + \overline{\hat{\eta}}_{\mathrm{FD}}(\phi)],\end{aligned} \tag{2.10a}$$

where

$$H(\phi,\psi,\rho,\eta,\xi,\mathcal{G}) = \coth\phi - \frac{\rho}{\sinh\phi} - h(\phi,\psi,\eta,\xi,\mathcal{G}) \tag{2.10b}$$

and

$$\hat{\Pi}_{44}^{(\mathrm{vac})}(0,\vec{\hat{k}}) = -N_f g^2\int_{-\pi}^{\pi}\frac{d^3\hat{p}}{(2\pi)^3}H(\phi,\psi,\rho,\eta,\xi,\mathcal{G}) \tag{2.10c}$$

is the $T=\mu=0$ contribution. As we now show, $\hat{\Pi}_{44}^{(\mathrm{vac})}(0,\vec{\hat{k}})$ vanishes in the limit $\vec{\hat{k}}\to 0$, and hence does not contribute to the screening mass.

Consider the function $h(\phi,\psi,\eta,\xi,\mathcal{G})$ defined in Eq. (2.6b). It is singular for $\vec{\hat{k}}\to 0$, since in this limit $\psi\to\phi$. The singularity is, however, integrable.[1] This can be seen as follows. Since according to Eq. (2.5), and the statement following it,

[1] We follow here and in the following a technique used in Ref. [12], where the author has calculated the screening mass for naive fermions in lattice QED to one-loop order.

$$h(\phi,\psi,\eta,\xi,\mathcal{G}) \xrightarrow{\vec{p}\to-\vec{p}-\vec{k}} h(\psi,\phi,\eta,\xi,\mathcal{G}), \tag{2.11}$$

we can also write Eq. (2.10c) in the form

$$\hat{\Pi}_{44}^{(\mathrm{vac})}(0,\vec{k}) = -N_f g^2 \int_{-\pi}^{\pi} \frac{d^3\hat{p}}{(2\pi)^3}\left(\coth\phi - \frac{\rho}{\sinh\phi}\right) + \frac{1}{2}N_f g^2 \int_{-\pi}^{\pi} \frac{d^3\hat{p}}{(2\pi)^3}\,\tilde{h}(\phi,\psi,\eta,\xi,\mathcal{G}), \tag{2.12a}$$

where

$$\tilde{h}(\phi,\psi,\eta,\xi,\mathcal{G}) = h(\phi,\psi,\eta,\xi,\mathcal{G}) + h(\psi,\phi,\eta,\xi,\mathcal{G}). \tag{2.12b}$$

Although each term on the RHS of Eq. (2.12b) is singular for $\vec{k}\to 0$ ($\psi\to\phi$), the sum possesses a finite limit. Thus setting $\psi=\phi+\epsilon$ and taking the limit $\vec{k}\to 0$ ($\epsilon\to 0$), one verifies that

$$\lim_{\vec{k}\to 0} \tilde{h}(\phi,\psi,\eta,\xi,\mathcal{G}) = 2\left(\coth\phi - \frac{\rho}{\sinh\phi}\right). \tag{2.13}$$

From Eq. (2.12a) we therefore conclude that

$$\lim_{\vec{k}\to 0} \hat{\Pi}_{44}^{(\mathrm{vac})}(0,\vec{k}) = 0.$$

This result is not unexpected, since for vanishing temperature and chemical potential it is well known in the continuum formulation that Lorentz and gauge invariance protects the gluon from acquiring a mass. The screening mass is therefore determined by the finite temperature (FT), finite chemical potential contribution, given by the integral in Eq. (2.10a). By making again use of the fact that $\phi\leftrightarrow\psi$, when $\vec{p}\to-\vec{p}-\vec{k}$, while η, ξ, and $\mathcal{G}$ remain invariant under this change of variables, we can write this contribution in the form

$$\begin{aligned}\hat{\Pi}_{44}^{(\beta,\mu)}(0,\vec{k})_{\mathrm{FT}} &= N_f g^2 \int_{-\pi}^{\pi} \frac{d^3\hat{p}}{(2\pi)^3}\left(\coth\phi - \frac{\rho}{\sinh\phi}\right)[\,\hat{\eta}_{\mathrm{FD}}(\phi) + \overline{\hat{\eta}}_{\mathrm{FD}}(\phi)] - \frac{1}{2}N_f g^2 \int_{-\pi}^{\pi} \frac{d^3\hat{p}}{(2\pi)^3}\{h(\phi,\psi,\eta,\xi,\mathcal{G}) \\ &\times[\,\hat{\eta}_{\mathrm{FD}}(\phi) + \overline{\hat{\eta}}_{\mathrm{FD}}(\phi)] + h(\psi,\phi,\eta,\xi,\mathcal{G})[\,\hat{\eta}_{\mathrm{FD}}(\psi) + \overline{\hat{\eta}}_{\mathrm{FD}}(\psi)]\}.\end{aligned} \tag{2.14}$$

Consider the second integral. It can be rewritten as follows:

$$\int_{-\pi}^{\pi} \frac{d^3\hat{p}}{(2\pi)^3}\{\tilde{h}(\phi,\psi,\eta,\xi,\mathcal{G})[\,\hat{\eta}_{\mathrm{FD}}(\psi) + \overline{\hat{\eta}}_{\mathrm{FD}}(\psi)] + h(\phi,\psi,\eta,\xi,\mathcal{G})\Delta\,\hat{\eta}_{\mathrm{FD}}(\phi,\psi)\},$$

where $\tilde{h}$ has been defined in Eq. (2.12b), and

$$\Delta\,\hat{\eta}_{\mathrm{FD}}(\phi,\psi) = [\,\hat{\eta}_{\mathrm{FD}}(\phi) - \hat{\eta}_{\mathrm{FD}}(\psi)] + [\,\overline{\hat{\eta}}_{\mathrm{FD}}(\phi) - \overline{\hat{\eta}}_{\mathrm{FD}}(\psi)].$$

According to Eq. (2.13), $\tilde{h}$ approaches a finite limit for $\vec{k}\to 0$. Upon making the change of variables $\vec{p}\to-\vec{p}-\vec{k}$ the contribution proportional to $\tilde{h}$ is seen to be canceled by the first integral in Eq. (2.14). We therefore conclude that

$$\lim_{\vec{k}\to 0} \hat{\Pi}_{44}^{(\beta,\mu)}(0,\vec{k}) = -\frac{1}{2}N_f g^2 \lim_{\vec{k}\to 0} \int_{-\pi}^{\pi} \frac{d^3\hat{p}}{(2\pi)^3} \times h(\phi,\psi,\eta,\xi,\mathcal{G})\Delta\,\hat{\eta}_{\mathrm{FD}}(\phi,\psi). \tag{2.15}$$

We have now dropped the subscript ''FT,'' since in this limit only Eq. (2.14) contributes to the screening mass. To calculate this limit we proceed as before and set $\psi=\phi+\epsilon$. One then verifies that for $\epsilon\to 0$ (or $\vec{k}\to 0$) the fermionic contribution to the screening mass squared is given by

$$[\hat{m}_{\mathrm{el}}^2(\hat{\beta},\hat{\mu},\hat{m})]_{\mathrm{ferm}} = N_f g^2 \hat{\beta} \int_{-\pi}^{\pi} \frac{d^3\hat{p}}{(2\pi)^3}\left\{\frac{e^{\hat{\beta}(\phi+\hat{\mu})}}{[e^{\hat{\beta}(\phi+\hat{\mu})}+1]^2} + \frac{e^{\hat{\beta}(\phi-\hat{\mu})}}{[e^{\hat{\beta}(\phi-\hat{\mu})}+1]^2}\right\}. \tag{2.16}$$

In the continuum limit the electric screening mass is given by

$$m_{\mathrm{el}}^2 = \lim_{a\to 0} \frac{1}{a^2}\,\hat{m}_{\mathrm{el}}^2\left(\frac{\beta}{a},\mu a, ma\right). \tag{2.17}$$

For Wilson fermions, only momenta $\vec{p}$ in the immediate neighborhood of $\vec{p}=0$ contribute to the integral (2.16) for $\hat{\beta}\to\infty$, $\hat{\beta}\hat{\mu}=\beta\mu$, $\hat{\beta}\hat{m}=\beta m$ fixed. But in this limit $\hat{\beta}\phi(\vec{\hat{p}})\to\beta\sqrt{\vec{p}^2+m^2}$. Introducing in Eq. (2.16) the dimensioned momenta $\vec{p}=\vec{\hat{p}}/a$ as new integration variables, with a the lattice spacing, one then verifies, after performing the angular integration, and a partial integration that

$$[m_{\mathrm{el}}^2]_{\mathrm{ferm}} = N_f \frac{g^2}{2\pi^2}\int_0^{\infty} dp\,\frac{2p^2+m^2}{\sqrt{p^2+m^2}}[\,\eta_{\mathrm{FD}}(E,\mu) + \overline{\eta}_{\mathrm{FD}}(E,\mu)], \tag{2.18}$$

where $E=\sqrt{\vec{p}^2+m^2}$, and

$$\eta_{\mathrm{FD}}(E,\mu) = \frac{1}{e^{\beta(E-\mu)}+1}, \quad \overline{\eta}_{\mathrm{FD}}(E,\mu) = \frac{1}{e^{\beta(E+\mu)}+1} \tag{2.19}$$

are the Fermi-Dirac distribution functions for particles and antiparticles.

We next consider the contribution to the electric screening mass arising from diagrams (c)–(g) in Fig. 1. They only involve sums over Matsubara frequencies of the bosonic type. Since in the continuum limit the only dimensioned scale is the temperature, their contribution to the screening mass will be of the form const$\times gT$. For finite lattice spacing,

however, the temperature dependence will be modified by lattice artifacts. In the following we first consider diagrams (c)–(e) which have an analogue in the continuum.

C. Contribution of diagram (c)

Using the lattice Feynman rules given in Appendix A one finds after some algebra that this diagram contributes as follows to $\hat{\Pi}_{44}^{(\beta,\mu)}(0,\vec{k})$, defined in Eq. (2.1),

$$\hat{\Pi}_{44}^{(\beta,\mu)}(0,\vec{k})_{(c)}=\frac{3}{2}g^2\frac{1}{\hat{\beta}}\sum_{l=-\hat{\beta}/2}^{\hat{\beta}/2-1}\int_{-\pi}^{\pi}\frac{d^3\hat{q}}{(2\pi)^3}f^{(c)}(e^{i\hat{\omega}_l^+};\vec{\hat{q}},\vec{k}), \tag{2.20a}$$

where

$$f^{(c)}(z;\vec{\hat{q}},\vec{k})=\frac{a(\vec{\hat{k}})(z^2-1)^2-b(\vec{\hat{q}},\vec{\hat{k}})z(z+1)^2}{\Pi_{i=1}^4[z-\overline{z_i}]} \tag{2.20b}$$

and

$$a(\vec{\hat{k}})=\sum_j\cos^2\frac{\hat{k}_j}{2}, \tag{2.20c}$$

$$b(\vec{\hat{q}},\vec{\hat{k}})=\frac{1}{4}\left[\sum_j\widetilde{(\hat{q}-\hat{k})}_j^2+\sum_j\widetilde{(\hat{q}+2\hat{k})}_j^2\right]. \tag{2.20d}$$

Here $\tilde{\hat{p}}$ is generically defined by $\tilde{\hat{p}}_\mu=2\sin(\hat{p}_\mu/2)$. The zeros of the denominator in Eq. (2.20b) are located at

$$\overline{z_1}=e^{\tilde{\phi}},\quad \overline{z_2}=e^{-\tilde{\phi}},$$
$$\overline{z_3}=e^{\tilde{\psi}},\quad \overline{z_4}=e^{-\tilde{\psi}}, \tag{2.21a}$$

where

$$\tilde{\phi}=\operatorname{arcosh}H(\vec{\hat{q}}),$$
$$\tilde{\psi}=\operatorname{arcosh}H(\vec{\hat{q}}+\vec{\hat{k}}),$$
$$H(\vec{\hat{p}})=1+2\sum_j\sin^2\frac{\hat{p}_j}{2}. \tag{2.21b}$$

The frequency sum can be calculated by making use of Eq. (B1). After some straightforward algebra one finds that

$$\hat{\Pi}_{44}^{(\beta,\mu)}(0,\vec{k})_{(c)}=6g^2\int_{-\pi}^{\pi}\frac{d^3\hat{q}}{(2\pi)^3}h(\tilde{\phi},\tilde{\psi},a,b)\,\hat{\eta}_{BE}(\tilde{\phi})+\frac{3}{2}g^2\left\{a(\vec{\hat{k}})+\int_{-\pi}^{\pi}\frac{d^3\hat{q}}{(2\pi)^3}[h(\tilde{\phi},\tilde{\psi},a,b)+h(\tilde{\psi},\tilde{\phi},a,b)]\right\}, \tag{2.22a}$$

where

$$h(\tilde{\phi},\tilde{\psi},a,b)=\frac{-a\sinh^2\tilde{\phi}+\frac{1}{2}b[\cosh\tilde{\phi}+1]}{\sinh\tilde{\phi}[\cosh\tilde{\phi}-\cosh\tilde{\psi}]} \tag{2.22b}$$

and

$$\hat{\eta}_{BE}(\tilde{\phi})=\frac{1}{e^{\hat{\beta}\tilde{\phi}}-1} \tag{2.22c}$$

is the lattice version of the Bose-Einstein distribution function.

In obtaining this result we have made use of the fact that

$$\tilde{\phi}\quad\overset{\vec{\hat{q}}\to-\vec{\hat{q}}-\vec{\hat{k}}}{\longleftrightarrow}\quad\tilde{\psi}, \tag{2.23}$$

while $a(\vec{\hat{k}})$ and $b(\vec{\hat{q}},\vec{\hat{k}})$ are invariant under the transformation $\vec{\hat{q}}\to-\vec{\hat{q}}-\vec{\hat{k}}$. Note that the function (2.22b) is singular for $\vec{\hat{k}}\to0$, since in this limit $\tilde{\phi}\to\tilde{\psi}$. The singularity is, however, integrable as can be seen by making use of Eq. (2.23) to write Eq. (2.22a) in the form

$$\hat{\Pi}_{44}^{(\beta,\mu)}(0,\vec{k})_{(c)}=3g^2\int_{-\pi}^{\pi}\frac{d^3\hat{q}}{(2\pi)^3}h(\tilde{\phi},\tilde{\psi},a,b)\Delta\hat{\eta}_{BE}(\tilde{\phi},\tilde{\psi})+\frac{3}{2}g^2\left\{a(\vec{\hat{k}})+\int_{-\pi}^{\pi}\frac{d^3\hat{q}}{(2\pi)^3}[h(\tilde{\phi},\tilde{\psi},a,b)+h(\tilde{\psi},\tilde{\phi},a,b)][1+2\hat{\eta}_{BE}(\tilde{\phi})]\right\}, \tag{2.24a}$$

where

$$\Delta\hat{\eta}_{BE}(\tilde{\phi},\tilde{\psi})=\hat{\eta}_{BE}(\tilde{\phi})-\hat{\eta}_{BE}(\tilde{\psi}). \tag{2.24b}$$

The limit $\vec{\hat{k}}\to0$ can now be easily taken and one obtains the following contribution to the electric screening mass:

$$(\hat{m}_{el}^2)_{(c)}=\frac{3}{2}g^2\left\{3-\int_{-\pi}^{\pi}\frac{d^3\hat{q}}{(2\pi)^3}\left[3\coth\tilde{\phi}+\frac{1}{2\sinh\tilde{\phi}}\right]\times[1+2\hat{\eta}_{BE}(\tilde{\phi})]\right\}+\frac{15}{2}g^2\hat{\beta}\times\int_{-\pi}^{\pi}\frac{d^3\hat{q}}{(2\pi)^3}\frac{e^{\hat{\beta}\tilde{\phi}}}{[e^{\hat{\beta}\tilde{\phi}}-1]^2}. \tag{2.25}$$

D. Contribution of diagram (d)

This diagram involves the 4-gluon vertex, which consists of types of terms differing in the color structure: terms involving the structure constants f_{ABC} and terms involving the completely symmetric color couplings d_{ABC}. We denote the corresponding contributions to $\hat{\Pi}_{44}^{(\beta,\mu)}(\hat{k})$ by $[\hat{\Pi}_{44}^{(\beta,\mu)}(\hat{k})]_{[f]}$ and $[\hat{\Pi}_{44}^{(\beta,\mu)}(\hat{k})]_{[d]}$, respectively. Consider first $[\hat{\Pi}_{44}^{(\beta,\mu)}(0,\vec{\hat{k}})_{(d)}]_{[f]}$. After some algebra one finds that

$$[\hat{\Pi}_{44}^{(\beta,\mu)}(0,\vec{\hat{k}})_{(\mathrm{d})}]_{[f]}=\frac{3}{4}g^2\frac{1}{\hat{\beta}}\sum_{l=-\hat{\beta}/2}^{\hat{\beta}/2-1}\int_{-\pi}^{\pi}\frac{d^3\hat{q}}{(2\pi)^3}\times[f^{(\mathrm{d})}(e^{i\hat{\omega}_l^+};\hat{q},\hat{k})]_{[f]}, \tag{2.26a}$$

where

$$[f^{(\mathrm{d})}(z;\vec{\hat{q}},\vec{\hat{k}})]_{[f]}=\frac{-c(\vec{\hat{k}})(z^2+1)+d(\vec{\hat{k}})(z-1)^2+P(\vec{\hat{q}},\vec{\hat{k}})z}{[z-\overline{z_1}][z-\overline{z_2}]} \tag{2.26b}$$

and

$$c(\vec{\hat{k}})=1+2\sum_j\cos\hat{k}_j,$$

$$d(\vec{\hat{k}})=1-\frac{1}{3}\sum_j\tilde{\hat{k}}_j^2,$$

$$P(\vec{\hat{q}},\vec{\hat{k}})=2+\frac{1}{6}\sum_j[(\widetilde{\hat{q}+\hat{k}})_j^2+(\widetilde{\hat{q}-\hat{k}})_j^2]. \tag{2.26c}$$

Performing the frequency sum in Eq. (2.26a) one obtains

$$[\hat{\Pi}_{44}^{(\beta,\mu)}(0,\vec{\hat{k}})_{(\mathrm{d})}]_{[f]}=\frac{3}{4}g^2\left\{-c(\vec{\hat{k}})+d(\vec{\hat{k}})+\int_{-\pi}^{\pi}\frac{d^3\hat{q}}{(2\pi)^3}\times\left[(c-d)\coth\tilde{\phi}+\left(d-\frac{1}{2}P\right)\times\frac{1}{\sinh\tilde{\phi}}\right][1+2\hat{\eta}_{\mathrm{BE}}(\tilde{\phi})]\right\}. \tag{2.27}$$

Taking the limit $\vec{\hat{k}}\to 0$ one finds the following contribution to the screening mass:

$$(\hat{m}_{\mathrm{el}}^2)_{[f]}^{(\mathrm{d})}=\frac{1}{2}g^2\left\{-9+\frac{1}{2}\int_{-\pi}^{\pi}\frac{d^3\hat{q}}{(2\pi)^3}\left[17\coth\tilde{\phi}+\frac{1}{\sinh\tilde{\phi}}\right]\times[1+2\hat{\eta}_{\mathrm{BE}}(\tilde{\phi})]\right\}. \tag{2.28}$$

Next consider the contribution $[\hat{\Pi}_{44}^{(\beta,\mu)}(0,\vec{\hat{k}})_{(\mathrm{d})}]_{[d]}$. It is given by

$$[\hat{\Pi}_{44}^{(\beta,\mu)}(0,\vec{\hat{k}})_{(\mathrm{d})}]_{[d]}=-\frac{1}{2}g^2\frac{1}{\hat{\beta}}\sum_{l=-\hat{\beta}/2}^{\hat{\beta}/2-1}\int_{-\pi}^{\pi}\frac{d^3\hat{q}}{(2\pi)^3}\times[f^{(\mathrm{d})}(e^{i\hat{\omega}_l^+};\vec{\hat{q}},\vec{\hat{k}})]_{[d]}, \tag{2.29a}$$

where

$$[f^{(\mathrm{d})}(z;\vec{\hat{q}},\vec{\hat{k}})]_{[d]}=\frac{5}{6}\frac{K(\vec{\hat{k}})(z-1)^2-L(\vec{\hat{q}},\vec{\hat{k}})z}{[z-\overline{z_1}][z-\overline{z_2}]}, \tag{2.29b}$$

$$K(\vec{\hat{k}})=\sum_j\tilde{\hat{k}}_j^2, \tag{2.29c}$$

$$L(\vec{\hat{q}},\vec{\hat{k}})=\sum_j\tilde{\hat{q}}_j^2\tilde{\hat{k}}_j^2. \tag{2.29d}$$

Performing the frequency sum one finds

$$[\hat{\Pi}_{44}^{(\beta,\mu)}(0,\vec{\hat{k}})_{(\mathrm{d})}]_{[d]}=\frac{5}{12}g^2\left\{-K+\int_{-\pi}^{\pi}\frac{d^3\hat{q}}{(2\pi)^3}\left[K\coth\tilde{\phi}-\frac{K+\frac{1}{2}L}{\sinh\tilde{\phi}}\right][1+2\hat{\eta}_{\mathrm{BE}}(\tilde{\phi})]\right\}.$$

Since $K(\vec{\hat{k}})$ and $L(\vec{\hat{q}},\vec{\hat{k}})$ vanish for $\vec{\hat{k}}\to 0$, it does not contribute to the screening mass, i.e.,

$$[(\hat{m}_{\mathrm{el}})_{(\mathrm{d})}]_{[d]}=0. \tag{2.30}$$

E. Contribution of diagram (e)

The only other diagram possessing a continuum analogue is the ghost loop shown in Fig. 1(e). Its contribution is given by

$$\hat{\Pi}_{44}^{(\beta,\mu)}(0,\vec{\hat{k}})_{(\mathrm{e})}=\frac{3}{2}g^2\frac{1}{\hat{\beta}}\sum_{l=-\hat{\beta}/2}^{\hat{\beta}/2-1}\int_{-\pi}^{\pi}\frac{d^3\hat{q}}{(2\pi)^3}f^{(\mathrm{e})}(e^{i\hat{\omega}_l^+};\vec{\hat{q}},\vec{\hat{k}}), \tag{2.31a}$$

where

$$f^{(\mathrm{e})}(z;\vec{\hat{q}},\vec{\hat{k}})=-\frac{1}{2}\frac{(z^2-1)^2}{\Pi_{i=1}^4[z-\overline{z_i}]}. \tag{2.31b}$$

Performing the frequency sum one finds that

$$\hat{\Pi}_{44}^{(\beta,\mu)}(0,\vec{\hat{k}})_{(\mathrm{e})}=\frac{3}{4}g^2\left\{-1+\int_{-\pi}^{\pi}\frac{d^3\hat{q}}{(2\pi)^3}[g(\tilde{\phi},\tilde{\psi})+g(\tilde{\psi},\tilde{\phi})]+4\int_{-\pi}^{\pi}\frac{d^3\hat{q}}{(2\pi)^3}g(\tilde{\phi},\tilde{\psi})\hat{\eta}_{\mathrm{BE}}(\tilde{\phi})\right\}, \tag{2.32a}$$

where

$$g(\tilde{\phi},\tilde{\psi})=\frac{\sinh\tilde{\phi}}{\cosh\tilde{\phi}-\cosh\tilde{\psi}}. \tag{2.32b}$$

This function is again singular for $\vec{\hat{k}}\to 0$. To compute the limit we proceed as discussed earlier and write Eq. (2.32a) in the form

$$\hat{\Pi}_{44}^{(\beta,\mu)}(0,\vec{\hat{k}})_{(e)}=\frac{3}{4}g^2\Bigg\{-1+\int_{-\pi}^{\pi}\frac{d^3\hat{q}}{(2\pi)^3}[g(\tilde{\phi},\tilde{\psi})+g(\tilde{\psi},\tilde{\phi})]\times[1+2\,\hat{\eta}_{\rm BE}(\tilde{\phi})]+2\int_{-\pi}^{\pi}\frac{d^3\hat{q}}{(2\pi)^3}g(\tilde{\phi},\tilde{\psi})\Delta\,\hat{\eta}_{\rm BE}(\tilde{\phi},\tilde{\psi})\Bigg\},$$

where $\Delta\,\hat{\eta}_{\rm BE}(\tilde{\phi},\tilde{\psi})$ has been defined in Eq. (2.24b). Taking the limit $\vec{\hat{k}}\to 0$ one obtains

$$(\hat{m}_{\rm el}^2)_{(e)}=\frac{3}{4}g^2\Bigg\{-1+\int_{-\pi}^{\pi}\frac{d^3\hat{q}}{(2\pi)^3}[1+2\,\hat{\eta}_{\rm BE}(\tilde{\phi})]\coth\frac{\tilde{\phi}}{2}-2\hat{\beta}\int_{-\pi}^{\pi}\frac{d^3\hat{q}}{(2\pi)^3}\frac{e^{\hat{\beta}\tilde{\phi}}}{[e^{\hat{\beta}\tilde{\phi}}-1]^2}\Bigg\}. \tag{2.33}$$

Combining the results (2.25), (2.28), (2.30), and (2.33), we therefore find that those diagrams possessing a continuum analogue yield the following contribution to the electric screening mass in the gluonic sector:

$$(\hat{m}_{\rm el}^2)_{(c)+(d)+(e)}=g^2\Bigg\{-\frac{3}{4}+\frac{1}{2}\int_{-\pi}^{\pi}\frac{d^3\hat{q}}{(2\pi)^3}\Bigg(\coth\frac{\tilde{\phi}}{2}-\frac{1}{\sinh\tilde{\phi}}\Bigg)[1+2\,\hat{\eta}_{\rm BE}(\tilde{\phi})]\Bigg\}+6g^2\hat{\beta}\int_{-\pi}^{\pi}\frac{d^3\hat{q}}{(2\pi)^3}\frac{e^{\hat{\beta}\tilde{\phi}}}{[e^{\hat{\beta}\tilde{\phi}}-1]^2}. \tag{2.34}$$

The computation of the remaining contributions arising from diagrams (f) and (g), which are a consequence of the lattice regularization, is straightforward. One finds that they cancel the first term in Eq. (2.34). Hence the gluonic sector (G) contributes as follows to the screening mass:

$$[\hat{m}_{\rm el}^2(\hat{\beta},\hat{\mu},\hat{m})]_G=6g^2\hat{\beta}\int_{-\pi}^{\pi}\frac{d^3\hat{q}}{(2\pi)^3}\frac{e^{\hat{\beta}\tilde{\phi}}}{[e^{\hat{\beta}\tilde{\phi}}-1]^2}. \tag{2.35}$$

In the continuum limit (2.17) the corresponding expression for the (dimensioned) screening mass squared is given by

$$(m_{\rm el}^2)_G=\lim_{a\to 0}6g^2\beta\int_{-\pi/a}^{\pi/a}\frac{d^3q}{(2\pi)^3}\frac{e^{\beta\tilde{\phi}(a\vec{q})/a}}{[e^{\beta\tilde{\phi}(a\vec{q})/a}-1]^2}=\frac{3}{\pi^2}g^2\beta\int_0^{\infty}dq\,q^2\frac{e^{\beta q}}{[e^{\beta q}-1]^2},$$

where $q=|\vec{q}|$. After a partial integration this expression takes the form

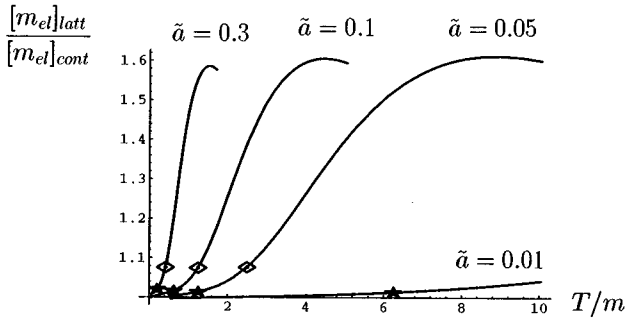

FIG. 2. Dependence of $[m_{\rm el}]_{\rm latt}/[m_{\rm el}]_{\rm cont}$ on T/m for $\mu=0$ and different lattice spacings measured in units of m^{-1}. Open squares (solid stars) correspond to lattices with $N_\tau=8$ ($N_\tau=16$).

$$(m_{\rm el}^2)_G=\frac{6}{\pi^2}g^2T^2\int_0^{\infty}dx\,\frac{x}{e^x-1}.$$

Making use of

$$\int_0^{\infty}dx\,\frac{x^{\alpha-1}}{e^x-1}=\Gamma(\alpha)\zeta(\alpha),\quad \alpha>1,$$

where $\Gamma(\alpha)$ is the Euler gamma function and $\zeta(\alpha)$ the Riemann zeta function, we recover the well-known result $(m_{\rm el}^2)_G=g^2T^2$.

III. LATTICE ARTIFACTS IN THE SCREENING MASS

In this section we compare the one-loop result for the electric screening mass on the lattice with the continuum. This will provide us with an estimate of the magnitude of the lattice artifacts to be expected in numerical simulations. The numerical data we present are for two mass-degenerate quarks.

On a lattice the temperature can be varied by either keeping the lattice spacing fixed and varying the number N_τ of temporal lattice sites or by varying the lattice spacing (or equivalently the coupling), keeping N_τ fixed. For fixed lattice spacing the dependence of the screening mass on the temperature, fermion mass, and chemical potential is given by [see Eq. (2.17)]

$$[m_{\rm el}(T,m,\mu,a)]_{\rm latt}=\frac{1}{a}\,\hat{m}_{\rm el}\Big(\frac{1}{Ta},\mu a,ma\Big). \tag{3.1}$$

If the lattice expression is to approximate the continuum, then the lattice spacing must be small compared to all physical length scales in the problem. Hence we must have that $a\ll 1/T$, $a\ll 1/m$, and $a\ll 1/\mu$. We therefore expect that for temperatures $T\ll 1/a$ the continuum is well approximated for $ma\ll 1$ and $\mu a\ll 1$. This is shown in Figs. 2 and 3 where we have plotted $[m_{\rm el}]_{\rm latt}/[m_{\rm el}]_{\rm cont}$ as a function of T/m at $\mu=0$ and $\mu/m=1.5$ for various lattice spacings measured in units of m^{-1}. For $\mu=0$ and $ma\equiv\tilde{a}\in[0,0.3]$, the deviation of this ratio from unity is seen to be at most 1.75% for $T/m\leqslant 1/16\tilde{a}$. The RHS of this inequality is the temperature associated with a lattice with 16 sites in the temporal direc-

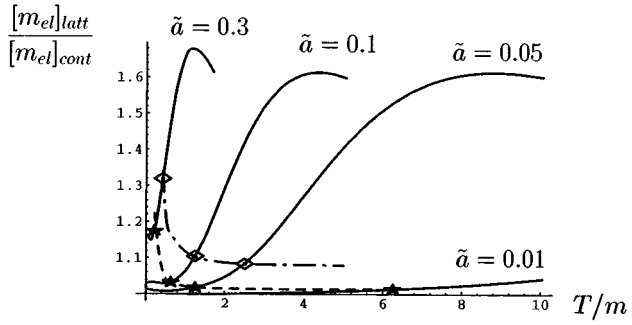

FIG. 3. Dependence of $[m_{\rm el}]_{\rm latt}/[m_{\rm el}]_{\rm cont}$ on T/m for $\mu/m=1.5$ and different lattice spacings measured in units of m^{-1}. Open squares (solid stars) correspond to lattices with $N_\tau=8$ ($N_\tau=16$). The dash-dotted (dashed) lines show the temperature dependence for a fixed number of temporal lattice sites, $N_\tau=8$ ($N_\tau=16$).

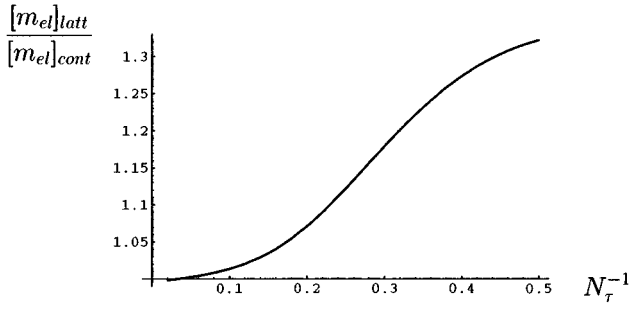

FIG. 4. Dependence of the pure gluonic contribution to $[m_{\rm el}]_{\rm latt}/[m_{\rm el}]_{\rm cont}$ on the number of lattice sites, N_τ. The solid line interpolates between different numbers of lattice sites, N_τ.

tion. For $T/m\approx 1/8\tilde{a}$ the deviation is already 7.5%. The end point of the curves for $\tilde{a}=0.05$, 0.1, and 0.3 corresponds to the minimal number of temporal lattice sites, i.e., $N_\tau=2$, and the open squares (solid stars) to $N_\tau=8$ ($N_\tau=16$).

For $\mu/m=1.5$ we must also ensure that $\mu a\ll 1$. We therefore expect that the allowed range of lattice spacings for achieving an accuracy of 2% for $T\leqslant 1/16a$ is now restricted to a smaller interval. Figure 3 shows that the continuum screening mass is well approximated for $\tilde{a}<0.1$ in this temperature range.

In lattice simulations one is interested in determining the electric screening mass above the deconfining phase transition. It is extracted from correlators of Polyakov loops [6–9] or from the long distance behavior of the gluon propagator [10]. In these simulations the number of lattice sites, $N_\tau\equiv\hat{\beta}$, is fixed. The electric screening mass in physical units, divided by the temperature, is then given by

$$[m_{\rm el}]_{\rm latt}/T=N_\tau\hat{m}_{\rm el}(N_\tau,(\mu/T)N_\tau^{-1},(m/T)N_\tau^{-1}), \quad (3.2)$$

while in the continuum limit ($N_\tau\to\infty$) this ratio is just a function of m/T and μ/T. The above conditions for approximating the continuuum now read (a) $N_\tau\gg 1$, (b) $ma=(m/T)\,(1/N_\tau)\ll 1$, and (c) $\mu a=(\mu/T)\,(1/N_\tau)\ll 1$. We therefore expect that for fixed N_τ the continuum is best approximated for high temperatures. For $\mu/m=1.5$ this is shown in Fig. 3, where the temperature dependence of $[m_{\rm el}]_{\rm latt}/[m_{\rm el}]_{\rm cont}$ for $N_\tau=8$ and $N_\tau=16$ is given by the dash-dotted and dashed curves, respectively. The strong deviation of this ratio at low temperatures is due to the fermion loop contribution. This is evident from Fig. 4, where we have plotted $[m_{\rm el}]_{\rm latt}/[m_{\rm el}]_{\rm cont}$ for the pure SU(3) gauge theory for various values of N_τ. This ratio only depends on the number of lattice sites, N_τ. The solid line interpolates between different numbers of temporal lattice sites. The deviation from the continuum is seen to be small already for $N_\tau=8$. For $N_\tau=8$, and $N_\tau=16$, it is about 2%, and 0.4%, respectively.

Finally, in Fig. 5 we have plotted the ratio $[m_{\rm el}]_{\rm latt}/[m_{\rm el}]_{\rm cont}$ as a function of m/T and μ/T for $N_\tau=8,16$. In the parameter range considered the above inequalities are well satisfied and the deviation of this ratio from unity is seen to be at most 1.7% for $N_\tau=16$ and 10% for $N_\tau=8$. The range of values m/T and μ/T for which the continuum is well approximated will of course increase with increasing N_τ.

IV. CONCLUSIONS

In this paper we have have computed the electric screening mass for Wilson fermions in the infinite volume limit for lattice QCD at finite temperature and chemical potential in one-loop order. The expression we obtained had a very transparent structure in which the artifacts arising from a finite lattice spacing were concentrated in two functions which in the naive continuum limit reduced to the on-shell energies of a free quark and gluon. We then studied the dependence of the lattice screening mass on the temperature and chemical potential for fixed values of the lattice spacing. It was found that lattice artifacts give rise to an enhancement of the screening mass. For $\mu=0$ and lattice spacings $a<0.3m^{-1}$ the deviation of $[m_{\rm el}]_{\rm latt}/[m_{\rm el}]_{\rm cont}$ from the continuum was found to be less than 1.75% for $T/m\leqslant 1/16\tilde{a}$, where $\tilde{a}=ma$. For $\mu/m=1.5$ a substantially smaller lattice spacing was required to approximate the continuum. Most of the deviation was found to be due to the fermion loop contribution.

Since in numerical simulations the temperature dependence of the screening mass is extracted from a given lattice by varying the coupling (lattice spacing), we have also studied the dependence of the lattice screening mass on the temperature and chemical potential for fixed N_τ. It was found that for $N_\tau=16$ and temperatures larger than the fermion mass and chemical potential, the continuum screening mass was approximated to within 1.75%. The corresponding deviation for $N_\tau=8$ was found to be at most 10% and to be due to the fermion loop contribution. In the pure SU(3) gauge theory the continuum was already approximated to 2% for only eight lattice sites in the temporal direction.

Our analysis was carried out for infinite lattice volume. For finite spatial volume the momentum spectrum becomes discrete and zero momentum modes must be treated separately in a perturbative expansion. In comparing the data for the electric screening mass obtained in Monte Carlo simulations with continuum perturbation theory, finite volume effects need to be included, while finite lattice spacing effects

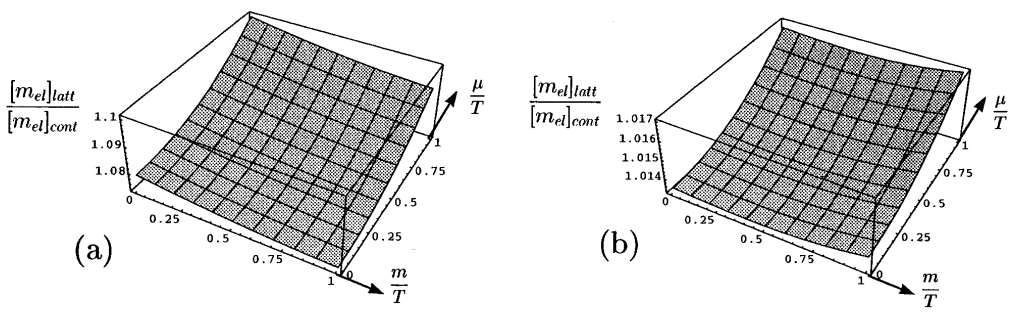

FIG. 5. Dependence of $[m_{\rm el}]_{\rm latt}/[m_{\rm el}]_{\rm cont}$ on m/T and μ/T for (a) $N_\tau=8$ and (b) $N_\tau=16$.

may, as our analysis suggests, be negligible for those couplings and lattice sizes at which the simulations have been performed.

ACKNOWLEDGMENTS

We are very grateful to T. Reisz for several discussions and constructive comments.

APPENDIX A: FEYNMAN RULES

For vanishing temperature and chemical potential the lattice Feynman rules have been given in [13]. The expression for the four-gluon vertex stated in that reference is, however, not quite correct. For completeness sake we collect in this appendix the Feynman rules for lattice QCD with Wilson fermions at finite temperature and chemical potential. In this case the fourth components of boson and fermion momenta are replaced by $k_4=\omega_\ell^+=2\pi\ell/\beta$ and $p_4=\omega_\ell^-+i\mu=(2\ell+1)\pi/\beta+i\mu$, respectively. As usual the gluon fields are defined at the middle of the links. Following standard conventions, we did not include the combinatorial factor arising from the symmetrization of the vertices. The dimensionless version of these rules, used in Sec. II, is obtained by setting $a=1$.

(i) Fermion, gauge field and ghost propagators:

$b,\beta \quad p \quad a,\alpha \qquad \delta_{ab}\,\dfrac{\left[-i/a\sum_\mu \gamma_\mu \sin(ap_\mu)+m(p)\right]_{\alpha\beta}}{1/a^2\sum_\mu \sin^2(ap_\mu)+m^2(p)}$

where

$$m(p)=m+\frac{2r}{a}\sum_\mu \sin^2\left(\frac{a}{2}p_\mu\right)$$

is the momentum-dependent Wilson mass and r the Wilson parameter which we have set to 1 in the calculation.

$B,\nu \quad k \quad A,\mu \qquad \delta_{AB}\frac{1}{\tilde{k}^2}\left[\delta_{\mu\nu}-(1-\lambda)\frac{\tilde{k}_\mu\tilde{k}_\nu}{\tilde{k}^2}\right] \quad ; \quad \tilde{k}_\mu=\frac{2}{a}\sin(\frac{a}{2}k_\mu)$

$B \quad k \quad A \qquad \delta_{AB}\frac{1}{\tilde{k}^2}$

(ii) The vertices:

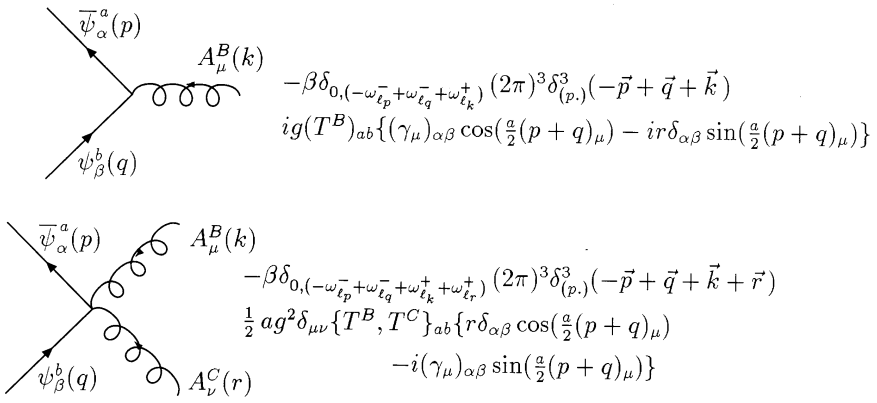

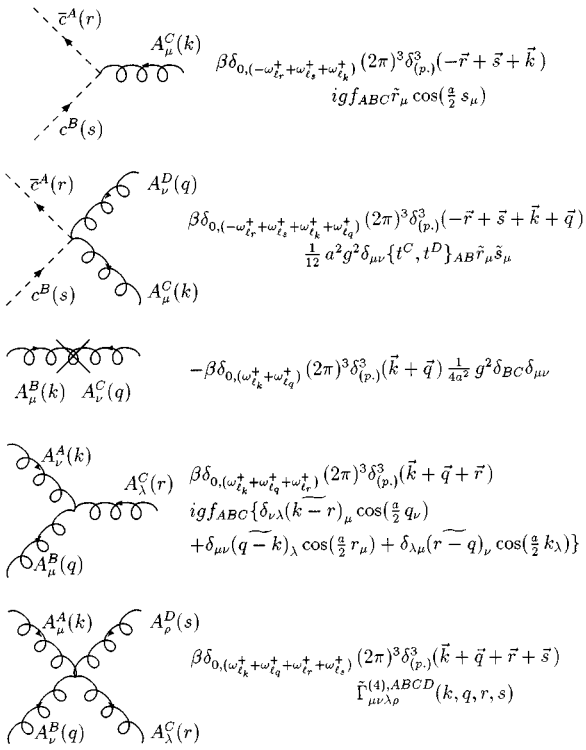

where

$$\widetilde{\Gamma}^{(4)ABCD}_{\mu\nu\lambda\rho}(k,q,r,s)=\frac{1}{12}g^2\Bigg[\Bigg(\sum_E f_{ABE}f_{CDE}\Bigg\{-\delta_{\mu\lambda}\delta_{\nu\rho}\Bigg[12\cos\Big(\frac{1}{2}a(k-r)_\nu\Big)\cos\Big(\frac{1}{2}a(q-s)_\mu\Big)-a^4\widetilde{k}_\nu\widetilde{q}_\mu\widetilde{r}_\nu\widetilde{s}_\mu\Bigg]$$

$$+\delta_{\mu\rho}\delta_{\nu\lambda}\Bigg[12\cos\Big(\frac{1}{2}a(k-s)_\nu\Big)\cos\Big(\frac{1}{2}a(q-r)_\mu\Big)-a^4\widetilde{k}_\nu\widetilde{q}_\mu\widetilde{r}_\mu\widetilde{s}_\nu\Bigg]-\delta_{\nu\lambda}\delta_{\nu\rho}2a^2(\widetilde{s-r})_\mu\widetilde{k}_\nu\cos\Big(\frac{1}{2}aq_\mu\Big)$$

$$+\delta_{\mu\lambda}\delta_{\mu\rho}2a^2(\widetilde{s-r})_\nu\widetilde{q}_\mu\cos\Big(\frac{1}{2}ak_\nu\Big)-\delta_{\mu\nu}\delta_{\mu\rho}2a^2(\widetilde{q-k})_\lambda\widetilde{r}_\rho\cos\Big(\frac{1}{2}as_\lambda\Big)$$

$$+\delta_{\mu\nu}\delta_{\mu\lambda}2a^2(\widetilde{q-k})_\rho\widetilde{s}_\lambda\cos\Big(\frac{1}{2}ar_\rho\Big)-\delta_{\mu\nu}\delta_{\mu\lambda}\delta_{\mu\rho}a^2\sum_\sigma(\widetilde{q-k})_\sigma(\widetilde{s-r})_\sigma\Bigg\}$$

$$+\text{ the cyclic permutations:}\begin{pmatrix}(B,q,\nu)&(C,r,\lambda)&(D,s,\rho)\\(C,r,\lambda)&(D,s,\rho)&(B,q,\nu)\end{pmatrix}\text{ and }\begin{pmatrix}(B,q,\nu)&(C,r,\lambda)&(D,s,\rho)\\(D,s,\rho)&(B,q,\nu)&(C,r,\lambda)\end{pmatrix}\Bigg)$$

$$+a^4\Bigg\{\frac{2}{3}(\delta_{AB}\delta_{CD}+\delta_{AC}\delta_{DB}+\delta_{AD}\delta_{BC})+\sum_E(d_{ABE}d_{CDE}+d_{ACE}d_{DBE}+d_{ADE}d_{BCE})\Bigg\}$$

$$\times\Bigg\{\delta_{\mu\nu}\delta_{\mu\lambda}\delta_{\mu\rho}\sum_\sigma\widetilde{k}_\sigma\widetilde{q}_\sigma\widetilde{r}_\sigma\widetilde{s}_\sigma+\delta_{\mu\nu}\delta_{\lambda\rho}\widetilde{k}_\lambda\widetilde{q}_\lambda\widetilde{r}_\mu\widetilde{s}_\mu+\delta_{\mu\lambda}\delta_{\nu\rho}\widetilde{k}_\nu\widetilde{q}_\mu\widetilde{r}_\nu\widetilde{s}_\mu+\delta_{\mu\rho}\delta_{\nu\lambda}\widetilde{k}_\nu\widetilde{q}_\mu\widetilde{r}_\mu\widetilde{s}_\nu$$

$$-\delta_{\nu\lambda}\delta_{\nu\rho}\widetilde{k}_\nu\widetilde{q}_\mu\widetilde{r}_\mu\widetilde{s}_\mu-\delta_{\mu\lambda}\delta_{\mu\rho}\widetilde{k}_\nu\widetilde{q}_\mu\widetilde{r}_\nu\widetilde{s}_\nu-\delta_{\mu\nu}\delta_{\mu\rho}\widetilde{k}_\lambda\widetilde{q}_\lambda\widetilde{r}_\mu\widetilde{s}_\lambda-\delta_{\mu\nu}\delta_{\mu\lambda}\widetilde{k}_\rho\widetilde{q}_\rho\widetilde{r}_\rho\widetilde{s}_\mu\Bigg\}\Bigg].$$

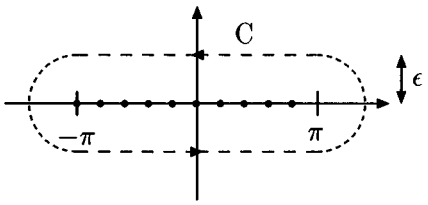

FIG. 6. Integration contour C in Eq. (B2).

APPENDIX B: FREQUENCY SUMMATION FORMULAS

In this appendix we derive summation formulas over Matsubara frequencies useful for performing calculations on a lattice, where the frequencies are restricted to the Brillouin zone. We will first consider the bosonic case and afterwards turn to the fermionic one.

1. Bosonic frequency sums

We will prove the following summation formula:

Let $g(z)$ be a meromorphic function of a complex variable z that is bounded for $|z|\to\infty$ and has no singularities on the circle $|z|=1$. Then

$$\frac{1}{\hat{\beta}}\sum_{n=-\hat{\beta}/2}^{\hat{\beta}/2-1} g(e^{i\hat{\omega}_n^+}) = -\sum_i \frac{\mathrm{Res}_{\overline{z_i}}((1/z)\,g(z))}{\overline{z_i}^{\hat{\beta}}-1}, \quad \text{(B1)}$$

where $\hat{\beta}$ is a positive even number, $\hat{\omega}_n^+ = 2\pi n/\hat{\beta}$ and $\mathrm{Res}_{\overline{z_i}}((1/z)\,g(z))$ denotes the residue of $(1/z)\,g(z)$ at the pole $\overline{z_i}$.

Consider the function

$$h(\hat{\omega}) = \frac{i\hat{\beta}}{\exp(i\hat{\beta}\hat{\omega})-1},$$

which has simple poles at $\hat{\omega}=\hat{\omega}_n^+$, $n\in Z$, with residue 1. Because of the above conditions on $g(z)$, there exists an $\epsilon>0$ such that $g(e^{i\hat{\omega}})$ has no singularities for $\mathrm{Im}(\hat{\omega}) \in[-\epsilon,\epsilon]$. Hence

$$\frac{1}{\hat{\beta}}\sum_{n=-\hat{\beta}/2}^{\hat{\beta}/2-1} g(e^{i\hat{\omega}_n^+}) = \frac{1}{2\pi}\oint_C d\hat{\omega}\, g(e^{i\hat{\omega}})\,\frac{1}{\exp(i\hat{\beta}\hat{\omega})-1}, \quad \text{(B2)}$$

where C is the integration contour depicted in Fig. 6. Introducing the variable $z=\exp(i\hat{\omega})$ we obtain

$$\frac{1}{\hat{\beta}}\sum_{n=-\hat{\beta}/2}^{\hat{\beta}/2-1} g(e^{i\hat{\omega}_n^+}) = \frac{1}{2\pi i}\sum_{j=1}^{2}\oint_{C_j} dz\,\frac{g(z)}{z}\,\frac{1}{z^{\hat{\beta}}-1}, \quad \text{(B3)}$$

where C_1 and C_2 are the contours shown in Fig. 7 with the integration carried out in the indicated sense.

Since $\lim_{|z|\to\infty} z^{-\hat{\beta}} g(z)=0$, we can distort the outer integration contour to infinity taking into account the singularities of $g(z)$ for $|z|>1$. In the case where $g(z)$ is a meromorphic function, Eq. (B1) follows immediately.

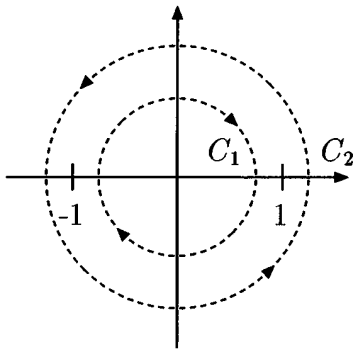

FIG. 7. Integration contours C_1 and C_2 in Eq. (B3).

2. Fermionic frequency sums

In the fermionic case we will proceed in an analogous way to prove the following summation formula [12].

Let $g(z)$ be a meromorphic function of a complex variable z that is bounded for $|z|\to\infty$ and has no singularities on the circle $|z|=\exp(-\hat{\mu})$. Then

$$\frac{1}{\hat{\beta}}\sum_{m=-\hat{\beta}/2}^{\hat{\beta}/2-1} g(e^{i(\hat{\omega}_m^- + i\hat{\mu})}) = \sum_i \frac{\mathrm{Res}_{\overline{z_i}}((1/z)\,g(z))}{e^{\hat{\beta}\hat{\mu}}\overline{z_i}^{\hat{\beta}}+1}, \quad \text{(B4)}$$

where $\hat{\omega}_m^- = (2m+1)\pi/\hat{\beta}$.

Consider the function

$$\tilde{h}(\hat{\omega}) = \frac{-i\hat{\beta}}{\exp[i\hat{\beta}(\hat{\omega}-i\hat{\mu})]+1},$$

which has simple poles at $\hat{\omega}=\hat{\omega}_m^- + i\hat{\mu}$, $m\in Z$, with residue 1. Because of the conditions on $g(z)$, there exists an $\epsilon>0$ such that $g(e^{i\hat{\omega}})$ has no singularities for $\mathrm{Im}(\hat{\omega}) \in[\hat{\mu}-\epsilon,\hat{\mu}+\epsilon]$. Hence

$$\frac{1}{\hat{\beta}}\sum_{m=-\hat{\beta}/2}^{\hat{\beta}/2-1} g(e^{i(\hat{\omega}_m^- + i\hat{\mu})}) = -\frac{1}{2\pi}\oint_C d\hat{\omega}\, g(e^{i\hat{\omega}}) \times\frac{1}{\exp[i\hat{\beta}(\hat{\omega}-i\hat{\mu})]+1}, \quad \text{(B5)}$$

where the integration contour C is depicted in Fig. 8. Introducing again the variable $z=\exp(i\hat{\omega})$ we obtain

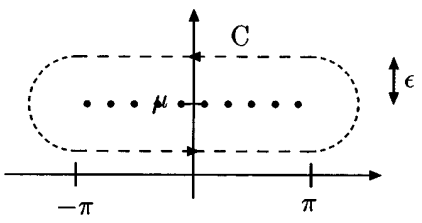

FIG. 8. Integration contour C in Eq. (B5).

$$\frac{1}{\hat{\beta}}\sum_{m=-\hat{\beta}/2}^{\hat{\beta}/2-1} g(e^{i(\hat{\omega}_m^- + i\hat{\mu})}) = -\frac{1}{2\pi i}\sum_{j=1}^{2}\oint_{C_j} dz\,\frac{g(z)}{z} \times \frac{1}{e^{\hat{\beta}\hat{\mu}} z^{\hat{\beta}} + 1},$$

where the integration contours C_1 and C_2 are as depicted in Fig. 7 except that the radii are changed to $e^{-\hat{\mu}-\epsilon}$ and $e^{-\hat{\mu}+\epsilon}$, respectively. Hence, for the same reason as in the bosonic case, we can distort the contour C_2 to infinity and are led, for a meromorphic function $g(z)$, to the summation formula (B4).

[1] O. K. Kalashnikov and V. V. Klimov, Yad. Fiz. **31**, 1357 (1980) [Sov. J. Nucl. Phys. **31**, 699 (1980)].

[2] A. K. Rebhan, Phys. Rev. D **48**, R3967 (1993); **52**, 2994 (1995); Nucl. Phys. **B430**, 319 (1994).

[3] A. D. Linde, Phys. Lett. **96B**, 289 (1980); see also D. Gross, R. Pisarski, and L. Yaffe, Rev. Mod. Phys. **53**, 43 (1981).

[4] E. Braaten and R. D. Pisarski, Phys. Rev. Lett. **64**, 1338 (1990); Nucl. Phys. **B337**, 567 (1990).

[5] R. Kobes, G. Kunstatter, and A. Rebhan, Phys. Rev. Lett. **64**, 2992 (1990); Nucl. Phys. **B355**, 1 (1991).

[6] M. Gao, Phys. Rev. D **41**, 626 (1990).

[7] A. Irbäk, P. LaCock, D. Miller, B. Petersson, and T. Reisz, Nucl. Phys. **B363**, 34 (1991).

[8] L. Kärkkäinen, P. LaCock, B. Peterson, and T. Reisz, Nucl. Phys. **B395**, 733 (1993).

[9] J. Engels, V. K. Mitrjushin, and T. Neuhaus, Nucl. Phys. **B440**, 555 (1995).

[10] U. M. Heller, F. Karsch, and J. Rank, Phys. Lett. B **355**, 511 (1995).

[11] B. Petersson and T. Reisz, Nucl. Phys. **B353**, 757 (1991).

[12] R. Pietig, Master thesis, Heidelberg, 1994 (unpublished).

[13] H. Kawai, R. Nakayama, and K. Seo, Nucl. Phys. **B189**, 40 (1981).